International Journal of Mass Spectrometry 438 (2019) 13–21

Contents lists available at ScienceDirect

International Journal of Mass Spectrometry

journal homepage: www.elsevier.com/locate/ijms

Full Length Article

Ionization probability of sputtered indium under irradiation with 20-keV fullerene and argon gas cluster projectiles

Andreas Wucher[a,*], Lars Breuer[a,b], Nicholas Winograd[b]

[a] Fakultät für Physik, Universität Duisburg-Essen, 47048, Duisburg, Germany
[b] The Pennsylvania State University, Department of Chemistry, 104 Chemistry Building, University Park, PA, 16802, USA

ARTICLE INFO

Article history:
Received 23 October 2018
Received in revised form
23 November 2018
Accepted 11 December 2018
Available online 14 December 2018

Keywords:
Cluster sputtering
Cluster ion bombardment
Ionization probability

ABSTRACT

The formation probability of secondary ions released from a metal surface under bombardment with a 20-keV cluster ion beam is investigated using combined time-of-flight secondary ion and neutral mass spectrometry (Tof-SIMS/SNMS) experiments. The emitted neutral atoms and clusters are post-ionized after their ejection using strong-field photoionization in an intense short infrared laser pulse. Comparing the secondary ion signal with that of the corresponding neutral particles, the ionization probability of sputtered indium atoms and In_n clusters with $n = 2–4$ is determined. The results are compared between two different projectile cluster ions, namely i) C_{60}^+ and ii) Ar_n^+ with $n \sim 1000$. It is shown that the ionization probability obtained with the fullerene cluster is by roughly a factor 4 larger than that obtained with the rare gas cluster, thereby indicating that there is no nonlinear enhancement of the transient electronic excitation generated by a cluster impact.

1. Introduction

Sputtering under polyatomic ion bombardment has received significant interest during recent years, because secondary ion yields produced by such species may be significantly larger than those produced by atomic projectiles of comparable impact energy. As a consequence, polyatomic ion bombardment using gold [1,2], bismuth [3–7], fullerene [8] or gas [9–11] cluster projectiles has now been implemented in routine time-of-flight secondary ion mass spectrometry (ToF-SIMS) analysis, since these projectiles generate significantly higher secondary ion yields at considerably less surface damage than monoatomic primary ions [12]. Particularly the advent of commercially available gas cluster ion beams (GCIB) consisting of consisting of up to thousands of atoms or molecules has opened new horizons in surface mass spectrometry, since these projectiles have been shown to allow a nearly fragment-free desorption of molecular species in some cases [13].

A fundamental open question regarding the role of projectile nuclearity (i. e., the number of constituent atoms of a projectile cluster) is whether the large secondary ion yield enhancements observed in many cases are due to an enhanced sputtering yield or an enhanced ionization of the sputtered species (or both). For the example of a clean metal surface, it is known that the flux of particles ejected under bombardment with a monoatomic ion beam such as Ar^+ mainly consists of neutral atoms and clusters, with the cluster yields being significantly smaller than that of the emitted atoms and decaying according to a power law with increasing cluster size [14–24]. The ionization probability, i.e., the probability of a sputtered particle to leave the surface as a positively or negatively charged secondary ion, is found to be small ($\sim 10^{-4}$) for sputtered atoms and increase with increasing size of an emitted cluster [22,23,25]. On the other hand, it is known that cluster projectiles deposit their energy closer to the surface than monoatomic projectiles, thereby generating a different particle ejection mechanism that leads to an enhanced total sputter yield, accompanied by an enhanced contribution of emitted molecular species [26–28]. An interesting question in that context is whether the increased subsurface energy density also leads to an enhanced ionization efficiency of the sputtered material. A study of secondary ions alone cannot provide a clear answer to that question. In order to unravel the emission and ionization processes, additional information on the yields of the respective neutral counterparts is needed. In previous work, we have established a method to measure the ionization probability of sputtered species by combining ToF SIMS with laser post-ionization secondary neutral mass spectrometry (SNMS), thereby detecting secondary ions and neutrals under otherwise the same experimental conditions. In a previous study, this technique was used to determine the ionization probability of indium atoms

* Corresponding author.
E-mail address: andreas.wucher@uni-due.de (A. Wucher).

https://doi.org/10.1016/j.ijms.2018.12.007
1387-3806/

and clusters sputtered from a polycrystalline indium surface under bombardment with Au_n, ($n = 1–5$) [29] and C_{60} [30] projectile ions. In this work, we extend the experiment to large argon gas cluster projectiles containing approximately 1000 atoms and compare the yields and ionization probabilities of indium atoms and clusters sputtered under these conditions with those obtained under C_{60}^+ bombardment.

2. Experimental

2.1. Instrumentation

The time-of-flight (ToF) mass spectrometer used in these experiments has been described in detail elsewhere [31]. In brief, the instrument comprises a 40 keV C_{60}^+ and a 20 keV gas cluster ion source (IOG C60-40 and GCIB 20, Ionoptika Ltd., Southampton, UK), a reflectron type mass spectrometer and a microchannel plate (MCP) detector equipped with a high transmission grid above the detector surface and post-acceleration capabilities. The two ion beams impinge onto the investigated sample surface under polar angles of 40° (GCIB) and 45° (C_{60}), respectively, with the azimuth angle between both beams being 135°, and are operated in pulsed mode. Both beams were focused to a spot size of approximately 30 μm and aligned to irradiate the same spot on the investigated sample. The latter was ensured by briefly bombarding the pristine indium sample with one beam in dc mode and then imaging the surface with the other beam operated in pulsed and rastered mode. Since the dc bombardment removes the native surface oxide, this results in a modified dark spot in the secondary ion image, which can then be used to overlap the two beams. The sample - consisting of a flat indium foil - was then pre-bombarded with the GCIB operated in dc mode with the Wien-filter switched off, thereby delivering a beam of predominantly atomic Ar^+ ions at about 10 nA current, which was rastered over an area of about 100×100 μm^2 for several minutes before the comparative spectra were taken with both ion beams operated in spot mode and pulsed. The ToF spectrometer is mounted with its ion optical axis along the sample surface normal and operated in the delayed extraction mode, where the sample is kept at ground potential during the primary ion pulse and switched to a positive potential of 2500 V afterwards, thereby generating the ion extraction field above the surface. The reflectron voltage was set at 6% less than the sample potential, thereby preventing ions starting directly at the surface from being reflected and detected. In connection with the time refocusing properties of the reflectron, this setting determines an effective ion extraction volume located above the surface, henceforth referred to as the *sensitive volume*, from which ions can be extracted and detected as described in detail elsewhere [32]. At the end of the primary ion pulse, ions present in the sensitive volume were swept into the ToF spectrometer by the pulsed extraction field as described above. While secondary ions could be directly detected, their neutral counterparts were post-ionized using a pulsed laser beam running parallel to the sample surface, which was overlapped with the sensitive volume and fired at a short delay (100 ns) after the ion extraction field. This way, the flight time zero is different for secondary ions (where it is defined by the start of the extraction pulse) and the post-ionized neutrals (where it is defined by the laser pulse). As a consequence, secondary ion and neutral peaks measured for particles of the same mass appear slightly displaced in the ToF spectrum, thereby allowing a clear distinction between both signals measured in the same spectrum as demonstrated below. Otherwise, the instrument cannot distinguish between intrinsic secondary ions and post-ionized neutrals, thereby allowing a quantitative comparison of the measured SIMS and SNMS spectra in order to determine the secondary ionization probability.

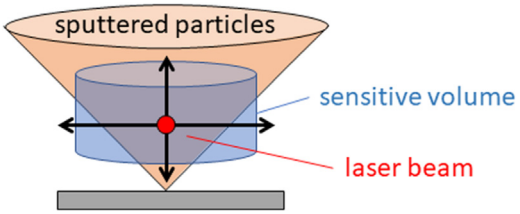

Fig. 1. Schematic view of the overlap between the plume of sputtered neutral particles, the sensitive volume of the mass spectrometer and the post-ionization laser beam. The laser was scanned along the indicated directions in order to map the detectable plume as defined in the text.

2.2. Laser system

Laser post-ionization (LPI) of sputtered neutral particles was performed with a commercially available chirped pulse amplification laser system (Coherent Legend Elite Duo, Santa Clara, CA, USA), providing 40 fs pulses of 800 nm radiation at a repetition rate of 1 kHz. The pulses were converted to mid-infrared radiation through an optical parametric amplifier (OPA) (Light Conversion TOPAS-C-HE, Vilnius, Lithuania), with wavelengths tunable from 1160 nm to 2580 nm. Experiments were performed at 1350 nm with a peak power of about 5×10^{14} W/cm^2 to ionize the sputtered neutral particles. The laser beam was introduced into the analysis chamber via a CaF_2 window and directed parallel to the sample surface at an azimuth angle of 38° or 175° with respect to the Ar_n^+ or C_{60}^+ primary ion beams, respectively. A 150 mm (at 587.6 nm) BK-7 focusing lens positioned outside the analysis chamber focuses the laser such that the beam waist approximately coincides with the location of the sensitive volume. The lens was translated in both the horizontal and vertical directions perpendicular to the direction of beam propagation in order to determine the optimal overlap with the sputtered material. After finding the optimal lateral position of the beam, the focusing lens was then translated along the beam propagation direction in order to defocus the beam such as to obtain the largest measured signal. As described in detail elsewhere [33], the laser intensity in the center of the beam then corresponds to the saturation intensity of the detected particles, and the beam diameter within the sensitive volume determines the effective ionization volume sampled by the laser. A power meter (Coherent Field Max II TO, Portland, OR) was used to measure the laser power as a 30 s average. The laser intensity in the focal volume was calibrated using xenon gas, which was introduced into the analysis chamber via a controllable leak valve and exhibits a well-known photoionization behavior as a function of the laser intensity [34].

At the beginning of each experiment, the position of the laser beam was optimized for maximum LPI signal. Due to the fact that the laser beam is tightly focused, the effective ionization volume sampled by the laser is significantly smaller than the extension of the sensitive volume. In fact, the cloud of principally detectable sputtered neutral molecules, henceforth referred to as the "detectable plume", has a dimension of the order of millimeters both along and perpendicular to the ion extraction axis, while the laser beam waist is of the order of several ten micrometers. As a consequence, the laser beam largely undersamples the detectable plume if kept at a fixed position. In order to investigate the magnitude of the this effect, the laser focusing lens was translated in 200 μm steps both horizontally and vertically with respect to the sample surface and SNMS spectra were recorded as a function of the laser beam position as indicated in Fig. 1. To account for possible signal loss as the experiment proceeds, for instance due to variations in laser power, the signals were measured at the optimal laser position again at the end of each experiment.

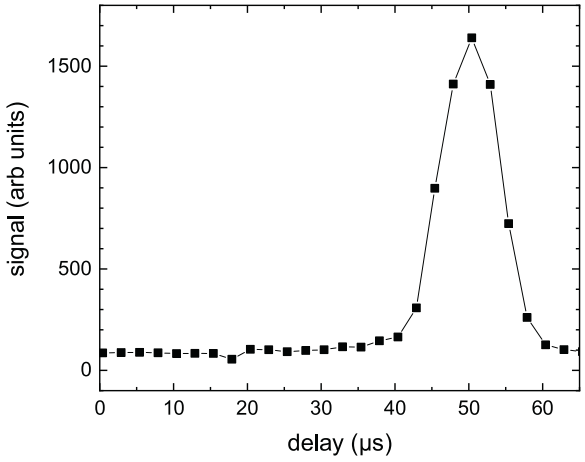

Fig. 2. Signal of post-ionized neutral indium atoms sputtered under bombardment with a 20-keV Ar_n^+ GCIB vs the delay between primary ion trigger pulse and data acquisition (marked by the time when both the ionizing laser and the ion extraction pulses are fired).

2.3. Timing considerations

A critical quantity needed for time-of-flight spectroscopy is the exact arrival time of the projectile ions at the sample surface. For the GCIB used here, the projectile mass is not uniquely fixed since the cluster beam contains a rather broad size distribution. As shown in the supplemental material, the ion beam employed in these experiments features a most probable cluster size of $n = 1050$ with a width of $\Delta n = \pm 200$ (FWHM) argon atoms. As a consequence, the timing of the ToF experiment needs to be adapted to the projectile arrival time distribution. In principle, it is possible to use a second pulser installed downstream of the ion source in order to select projectile ion clusters of a particular size [35]. This, however, leads to a significant reduction in the usable primary ion current and pulse width and therefore imposes a problem in the present work, since the experiments performed here rely on the detection of relatively small secondary ion signals in addition to those of post-ionized neutral particles. In addition, a short primary ion pulse leads to a restriction of the sampled velocity interval of the emitted secondary particles in a delayed extraction experiment as used here. We therefore chose to work with long primary ion pulses featuring the entire projectile cluster size distribution delivered by the GCIB. The relative timing needed to achieve optimum post-ionization signal is then found by scanning the delay between the primary ion trigger and the data acquisition time (i.e., the time when the laser and extraction pulses are being fired). An example of such a scan is shown in Fig. 2 for the In° signal of post-ionized neutral indium atoms emitted from an indium sample. Under the conditions employed here, with a 10 μs pulse triggering the GCIB, the measured curve essentially reflects the arrival time distribution of the projectile ions convoluted with the trigger pulse and therefore delivers the same information regarding the cluster size distribution as, for instance, the ion induced secondary electron signal.

In principle, the signals measured in the delayed extraction experiment as performed here represent the number density of secondary ions or post-ionized neutrals within the sensitive volume integrated over their emission velocity distribution. In order to distinguish post-ionization signals from those measured for the respective secondary ions, we will in the following refer to an ion originating from a post-ionized neutral species X as X°, whereas X^+ denotes the respective secondary ion. As described in detail in ref. [32], the upper limit of the velocity integral is determined by a possible delay between the end of primary ion pulse and the firing of the post-ionization laser and/or the ion extraction pulse. The lower limit of the integration interval is determined by the width of the primary ion pulse. Zero delay conditions can be identified by the signal maximum shown in Fig. 2, and the relative timing of primary ion and extraction pulses was set to ensure these conditions throughout the remainder of this work.

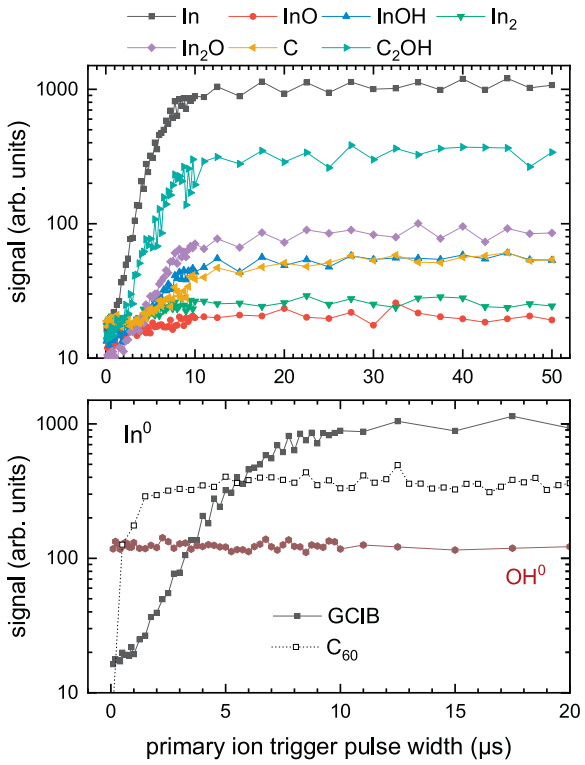

Fig. 3. Signal of post-ionized neutral atoms and molecules sputtered from a polycrystalline indium surface vs. temporal width of the primary ion trigger pulse. Upper panel: signals measured with a 20-keV Ar_n^+ GCIB; Bottom panel: indium atom signal measured with 20-keV Ar_n^+ and C_{60}^+ ion beams, respectively. For comparison, a residual gas signal measured at m/z 17 is included, which is independent of the primary ion bombardment.

The dependence of the measured signals on the width of the primary ion trigger pulse is shown in Fig. 3. With the exception of the neutral OH radical signal detected at m/z 17 (which arises from laser ionization of the residual gas and therefore is independent of the primary ion bombardment), all signals rise with increasing primary ion pulse width and reach a plateau value at sufficiently long ion pulses, indicating that particles of all relevant emission velocities are being detected. The shape of the rising edge constitutes a convolution of the neutral particle emission velocity distribution and the primary ion arrival time distribution. The bottom panel shows the same measurement for the In° signal detected under C_{60}^+ ion impact, where it is seen that the broadening induced by the emission velocity distribution is relatively small. Therefore, the curves measured under GCIB impact basically reflect the integrated primary ion arrival time distribution again. Using the 90%-10% transition of the GCIB-induced In° signal, we find a FWHM of about 8 μs which corroborates the conclusion drawn from the data in Fig. 2.

3. Results and discussion

The goal of the present work is to compare the mass spectra and the ionization efficiency of sputtered atoms and molecules induced by the two different projectile clusters. In that context, we define the ionization probability of a sputtered species X as

$$\alpha_X^{+,-} = \frac{Y_{X^{+,-}}}{Y_X} = \frac{Y_{X^{+,-}}}{Y_{X^0} + Y_{X^+} + Y_{X^-}}, \quad (1)$$

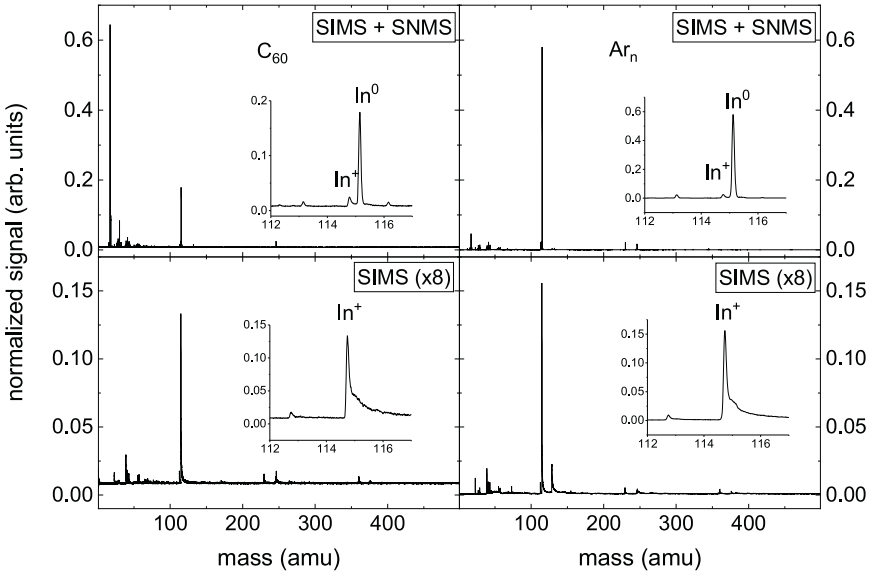

Fig. 4. Mass spectra measured for bombardment of a polycrystalline indium surface with 20 keV C_{60}^+ (left column) and Ar_{1000}^+ (right column) cluster projectiles. Upper row: SNMS spectra measured with the post-ionization laser placed at optimum position; bottom row: SIMS spectra without the post-ionization laser being fired. The measured signals were normalized to the primary ion current (20 pA for C_{60} and 300 pA for GCIB).

where Y_X is the partial sputter yield of X regardless of its charge state, while $Y_{X^{+,-}}$ and Y_{X^0} denote the partial sputter yields of positively and negatively charged secondary ions X^+, X^- and neutrals X°, respectively. The mass spectrometric signals measured for secondary ions and post-ionized neutrals, on the other hand, reflect the respective sputter yields via

$$S\left(X^{+,-}\right) = I_p \cdot Y_X \cdot \alpha_X^{+,-} \cdot \eta_X^{+,-} \tag{2}$$

and

$$S\left(X^0\right) = I_p \cdot Y_X \cdot \left(1 - \alpha_X^+ - \alpha_X^-\right) \cdot \alpha_X^0 \cdot \eta_X^0 \tag{3}$$

where I_p and α_X^0 denote the primary ion current and the post-ionization probability for the sputtered neutrals, respectively. The quantity η_X describes an instrumental collection and detection factor which – for the case of post-ionized neutral particles – also includes the overlap between the ionization laser and the detectable plume. If the laser intensity is high enough, the photoionization process is driven into saturation, meaning that the laser samples 100% of all neutral particles within an effective ionization volume determined by the molecule-specific saturation intensity I_{sat}. As described in detail elsewhere [36], the value of I_{sat} can be determined from experiments with varying laser intensities, and the volume effectively probed by the laser can then be estimated from a simple barrier suppression photoionization model [30,32]. For the comparative experiments performed here, however, its exact value is not needed, since we are probing the same neutral particles released from the same surface under bombardment with different projectile ion beams. As long as both experiments are performed under exactly the same laser post-ionization conditions, the effective ionization volume will be the same regardless of the projectile ions used to eject the sputtered neutral particles.

The remainder of this paper is organized as follows. First, we analyze the mass spectra obtained with both projectiles and elucidate some significant differences regarding, the relative contribution of indium clusters in the sputtered flux. Then, we investigate the sampling efficiency of the post-ionization laser in order to map the sensitive volume of the mass spectrometer and determine the total signal of principally detectable post-ionized neutrals. This signal then represents the number density of sputtered neutral particles integrated over the entire sensitive volume, which can be compared with the corresponding SIMS signal representing the number density of secondary ions integrated over the same volume. The ion/neutral density ratio determined this way does not directly reflect the ionization probability, however, since the definition of $\alpha^{+,-}$ is based on the ratio of secondary ion and neutral yields, which, in turn, reflect the *flux* of sputtered particles. If the emission velocity distributions of secondary neutrals and ions were different, the density/flux conversion would be different for both particles, thereby influencing the measured ionization probability. A previous measurement of the emission velocity distributions of neutral In atoms and In^+ secondary ions sputtered under impact of monoatomic Ar^+ projectiles has revealed that the resulting correction can amount to about a factor two. Unfortunately, we cannot repeat the same experiment here, since the technique used to measure the emission velocity distributions ultimately requires the use of short primary ion pulses. While this is possible for sputtered neutrals (where the emission velocity is selected by a controlled delay between primary ion and post-ionizing laser pulse), it is not easily possible for the secondary ions.

3.1. Mass spectra

The spectra measured with both projectiles are shown in Figs. 4 and 5. In both cases, the post-ionization laser was positioned such as to produce optimum LPI signal. Note that this position is not necessarily equivalent for both projectiles (see below). The upper panels display the SNMS spectra which were measured with the ion beam and post-ionization laser on, while the bottom row displays the SIMS spectra measured with the post-ionization laser switched off. In principle, the SNMS spectra contain both the SIMS signals and the residual gas background which is measured with the ionization laser only. A close inspection reveals that the residual gas spectrum mainly consists of a prominent OH radical peak at m/z 17 and, in particular, does not contain any non-negligible contributions at masses above 100 amu.

All signals displayed in the figure were normalized to the respective primary ion current in order render them comparable in terms of the corresponding sputter yields. As a consequence of this normalization, residual gas signals which are independent of the

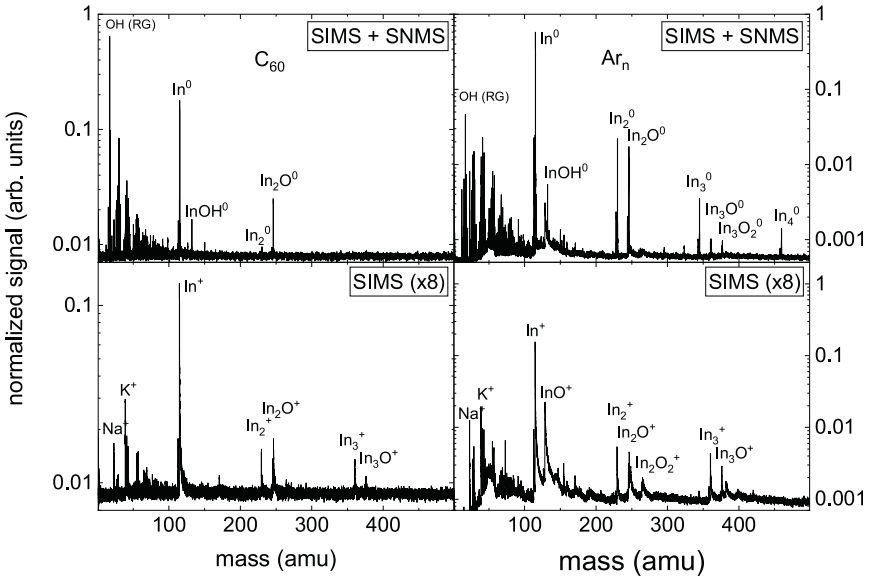

Fig. 5. Mass spectra shown in Fig. 4 plotted on a logarithmic scale.

projectile ion bombardment appear at different levels. This is the reason why the OH signal appears exaggerated the SNMS spectrum measured under C_{60} impact. If corrected for the current normalization, both signals visible at *m/z* 17 in the upper panels of Fig. 4 are of the same height. Among the sputtered particles, the signal of emitted neutral indium atoms by far dominates the measured spectra for both projectiles. The respective In° signal generated under Ar_n impact is by about a factor three larger than that generated by the iso-energetic C_{60} projectile, indicating an accordingly higher sputter yield for the gas cluster impact. The inserts in Fig. 4 show an expanded view around the indium atom mass. Since the post-ionization laser was slightly delayed with respect to the extraction pulse during acquisition of the SNMS spectra, the signals of secondary In^+ ions and neutral indium atoms appear displaced in the ToF spectrum, thereby allowing a clear distinction between both species. From the relative scaling of the In^+ and In° peaks observed in the SNMS spectra, it is evident that the ionization probability of sputtered indium atoms is small under irradiation with both cluster projectiles. The bottom panels show the SIMS spectra measured again with an increased detector gain setting, where the post-ionization laser was switched off in order to avoid signal saturation. It is seen that the normalized In^+ signal level is about the same in both spectra, indicating a similar secondary ion yield for both projectiles.

Apart from the sputtered atomic species, the mass spectra also contain signals of emitted indium clusters. This is visualized in Fig. 5, which shows the same mass spectra plotted on a logarithmic scale. In principle, cluster emission in sputtering of metallic surfaces is a well-documented phenomenon, and a body of corresponding yield data exists particularly for indium bombarded by various atomic and cluster projectiles. It was shown the neutral In_i clusters containing up to 200 atoms can be emitted under bombardment with atomic rare gas ions [18,23]. Irradiating the sample with small atomic silver [37,38], gold [39] or C_{60} [30] cluster ions, sputtered neutral indium clusters up to $i = 10$ have been detected, with the detection limit basically determined by the relatively low primary ion current achievable with the used cluster ion sources. In all cases, the yield distribution of the sputtered clusters was found to follow a power law according to $i^{-\delta}$, where the exponent δ varied between 3.9 and 5.6 depending on the bombarding conditions. Here, we find sputtered clusters containing up to 4 indium atoms under bombardment with the Ar_{1000} cluster projectile. If the

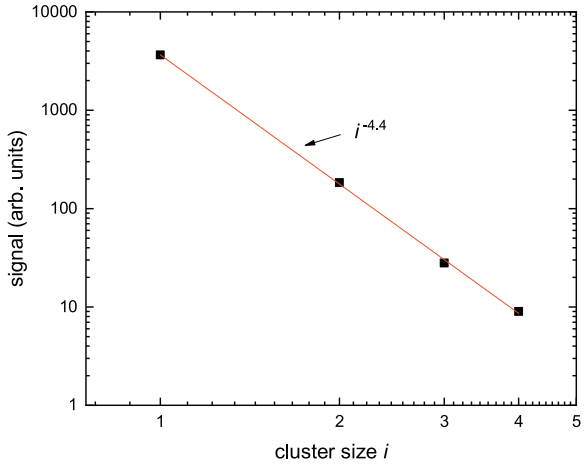

Fig. 6. Integrated signals of sputtered neutral In_i clusters produced under 20-keV Ar_{1000}^+-bombardment of a polycrystalline indium surface vs. cluster size i.

integrated In_i° signals are plotted vs. the cluster size *i*, they again reveal a power law with an exponent $\delta = 4.4$ as shown in Fig. 6. Under C_{60}^+ irradiation, the detection limit prevents the identification of clusters with $i > 2$ in Fig. 5, but in this case a previous experiment [30] performed on the same instrument also revealed a power law cluster size distribution with an exponent $\delta = 4.6$ under the same bombarding conditions as employed here. Since these values are close to the ones observed for 4-keV Ar ($\delta = 5.6$ [18]), 15-keV Xe ($\delta = 3.9$ [23]) and (5–10)-keV Au_n ($\delta = 4.3 - 5.7$ [39]) projectiles, we conclude that the yield distribution of sputtered clusters is essentially independent of the projectile. This finding is interesting, since the sputtering process initiated by a cluster impact was shown to be fundamentally different from that initiated by an isoenergetic atomic projectile both experimentally [40] and theoretically [27,28]. Under bombardment with atomic projectiles, particle ejection mainly occurs via a linear collision cascade, while a cluster impact generates a phase explosion of a super-critically heated (sub)surface volume [41]. Apparently, the cluster formation process among the sputtered material must be independent of the detailed ejection mechanism.

It should be noted that oxide molecules of the type In_iO_k are also observed in the mass spectra of Fig. 5, indicating that the

investigated indium surface was still slightly contaminated. These signals are most prominent for the indium dimer, with the In_2O° signal being of comparable magnitude as the In_2° signal for the gas cluster projectile. Under C_{60}^+ impact, on the other hand, the oxide signal is by far the dominant peak for the indium dimer, with its intensity amounting to about 14% of the monomer signal. This finding indicates that the argon cluster sputtering process may not be as sensitive to surface contamination as that induced by the C_{60} impact, for instance due to a different depth of origin distribution of the sputtered material. Another possible reason would be that the two ion beams are not exactly overlapped, so that the GCIB may have analyzed a slightly different surface spot than the C_{60} ion beam. On the other hand, the SIMS spectra show a prominent InO^+ peak under gas cluster bombardment, while no such peak is observed in the C_{60}-generated spectrum. Moreover, the In_iO^+/In_i^+ ratio is comparable for $i = 2–3$ between both projectiles, so that oxygen must clearly be present also in the Ar_{1000}^+-irradiated spot. In any case, the oxide signals constitute only minor components in the post-ionization spectra both for the indium monomers and all larger clusters containing more than two indium atoms.

3.2. Post-ionization efficiency

As explained above, the LPI signal measured with the focused ionization laser adjusted to a single position above the surface severely undersamples the plume of sputtered neutral particles that are in principle detectable by the post-ionization experiment. The SIMS signal, on the other hand, is generated by the entire detectable plume of secondary ions that are present above the surface at the time when the extraction field is switched on. A quantitative comparison with the corresponding post-ionization signal therefore requires to sample the entire detectable plume of neutral particles as well. For that purpose, the laser beam is scanned in directions parallel and perpendicular to the surface and the LPI signal is summed as described in detail elsewhere [30,33,42,43].

The resulting scans of the detectable neutral plume are shown in Fig. 7.

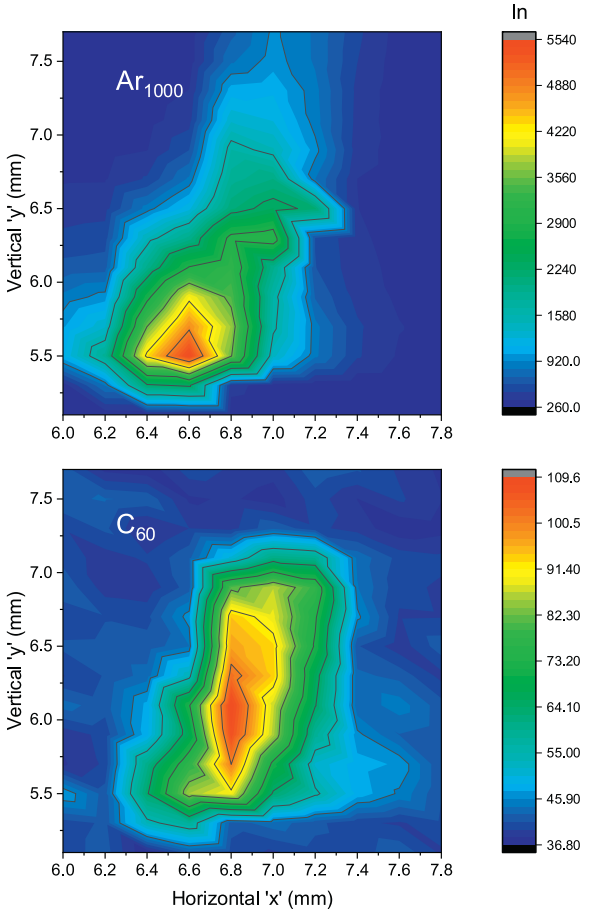

Fig. 7. Signal of post-ionized neutral indium atoms vs. lateral position of the ionizing laser beam for irradiation with 20-keV C_{60}^+ ions (bottom panel) and irradiation with 20-keV Ar_{1000}^+ ions (upper panel).

Summing the mass spectra measured at each laser position yields a total spectrum that is displayed in Fig. 8a). This spectrum can now be compared to that measured with the post-ionization laser positioned such as to obtain maximum LPI signal (Fig. 8b)) and the SIMS spectrum measured with the laser beam switched off (Fig. 8d)). The In° peak in panel a) reflects the hypothetical LPI spectrum which would be measured if the entire sensitive volume of the ToF spectrometer would be homogenously ionized by the laser. The In^+ secondary ion peak, on the other hand, is constant in all spectra and therefore appears greatly exaggerated in this plot. Subtracting the SIMS signal from all measured spectra, we obtain the summed LPI signal displayed in Fig. 8c). These spectra are interesting since they allow a discussion of the different peak shapes between LPI and SIMS that are observed in Fig. 5. As also seen in Fig. 8, all secondary ion peaks exhibit a tail towards longer flight times, which is not observed in the LPI peaks measured with a fixed post-ionization laser. The reason is that ions present in the upper parts of the sensitive volume at the time when the extraction field is fired enter the ToF spectrometer with smaller kinetic energy, leading to a shift of their flight time towards longer values. The measured SIMS spectrum always samples the entire sensitive volume, and therefore each secondary ion peak naturally contains the tail arising from these secondary ions. Secondary neutral particles post-ionized by the focused laser, on the other hand, originate from a well-defined position within the sensitive volume and therefore do not exhibit this tail. They do, however, shift in flight time once the laser beam is moved in the vertical direction. Summing the LPI spectra therefore simulates an LPI spectrum measured under comparable conditions as the SIMS spectrum. This is nicely observed in Fig. 8, where both the summed In° peak in panel c) and the In^+ peak in panel d) exhibit the same shape.

Looking at the data presented in Fig. 7, is apparent that the two distributions look quite different. Moreover, the optimum position of the laser beam generating the largest useable post-ionization signal is not the same under irradiation with both projectile ion beams. If the scan is performed for different signals generated by the same ion beam, on the other hand, the distributions look very similar (see Fig. 2 of the supporting material for neutral In_2 and In_3 clusters). Both findings are understandable, since the geometrical shape of the detectable plume depends on the emission angle and velocity distribution of the sputtered neutral particles, which will certainly depend on the projectile nature and impact angle. In fact, molecular dynamics computer simulations have shown that the polar emission angle distribution of sputtered metal atoms may drastically change with increasing projectile cluster size, with small clusters such as Ar_{60} leading to preferred emission along the surface normal, while larger clusters produce more pronounced off-normal emission with increasing cluster size [44]. Moreover, with both cluster projectiles impinging under 45° with respect to the surface normal, it is possible that the emission angle distribution may be forward-peaked in the plane of incidence of the respective ion beam, the effect again being more pronounced for the larger cluster [45]. Since both projectile beams form different azimuth angles with the ionizing laser beam (15° for C_{60}^+ and 60° for Ar_n^+), differences between the way the laser intersects the sputtered plume can be expected, where an off-normal emission would lead to a stronger laser displacement for the larger impact azimuth.

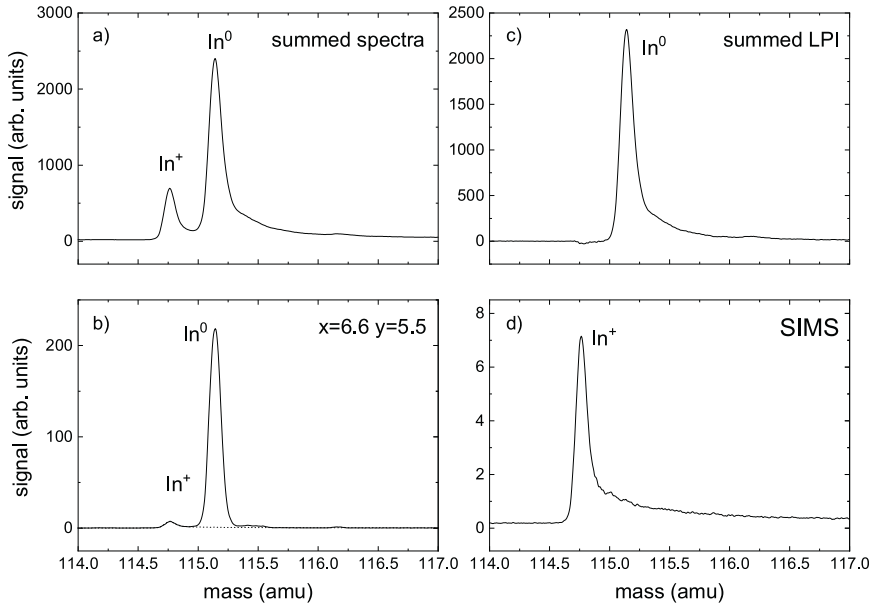

Fig. 8. Zoom of the GCIB-induced spectra: a) Summed signal of all SNMS spectra measured at the different post-ionization laser positions displayed in Fig. 7; b) SNMS spectrum measured with the post-ionization laser positioned such as to obtain maximum LPI signal; c) summed LPI spectra with SIMS signal subtracted; d) SIMS spectrum alone.

A second important observation is the apparent restriction of the sensitive volume in the vertical direction along the sample surface normal. In this context, it should be noted that lower y-values in Fig. 7 correspond to laser positions closer to the surface. The density of sputtered neutral particles continues to increase with decreasing distance r from the emission point. Without the geometrical restriction of the sensitive volume, the post-ionization signal would therefore continue to increase with decreasing height of the laser beam above the surface, until the laser finally hits the surface and starts to ablate material. The fact that the signal strongly decays below $y = 5.4$ mm therefore clearly demonstrates the restriction of the sensitive volume towards the surface, which is achieved by setting the reflection voltage below the stage potential. From the settings used here ($U_{\text{reflect}} = 0.94\ U_{\text{stage}}$) along with a distance of 12 mm between the surface and the extraction electrode, one would calculate that ions created below a minimum height of 0.7 mm above the surface cannot be reflected and detected. This would put the position of the surface at $y = 4.7$ mm in Fig. 7. Note, however, that any initial starting energy of the post-ionized neutrals would push this boundary upwards accordingly. In that context, the apparent differences in the vertical extension of the detectable plume might in principle indicate differences in the emission energy distribution of the sputtered particles, but further experiments or computer simulations would clearly be needed to substantiate this interpretation. In any case, the data presented in Fig. 7 clearly show that the entire detectable plume of sputtered neutral particles can be mapped.

The displayed distributions can therefore be summed to deliver the signal $S^0_{sum} = \sum_{i,j} S^0_{i,j}$, which is proportional to the (hypothetical) post-ionization signal integrated over the entire detectable plume. Relating this signal sum to the signal $S^0_{\max}$ measured with the laser beam set to a fixed laser position such as to deliver maximum signal, we find apparent sampling efficiency values listed in Table 1. Due to the low C_{60}^+ primary ion current used in these experiments, the signals measured for In_2 and In_3 were too small to arrive at meaningful data for these clusters under C_{60}^+ bombardment.

From the GCIB-induced data, it is evident that the effective sampling efficiency not only depends on the projectile ion beam, but may also vary for different measured signals. In order to determine the true sampling efficiency, the displayed values must be corrected by a factor $\nu = \pi[R']^2/(\Delta x \cdot \Delta y)$, where Δx and Δy represent the step size used in the laser beam scan and R' denotes the lateral diameter of the effective ionization volume sampled by the laser. The value of R' can be calculated from the parameters of the unfocused laser beam in connection with the saturation intensity of the detected neutral species as described in detail elsewhere [30]. Using the respective data measured for indium atoms and clusters [30], one can calculate that under optimized conditions the laser samples about 1–2 % of the detectable plume of sputtered neutral indium atoms and clusters. We stress, however, that the exact value of ν is not needed in order to compare the sampling efficiency between the two different projectile ions, provided the post-ionization conditions remain unchanged when switching between both primary ion beams.

Table 1
Ratio between signal of post-ionized indium atoms and clusters measured at optimized laser position and signal summed over the entire scans depicted in Fig. 7.

	In	In_2	In_3
C_{60}^+	0.042	–	–
Ar_n^+	0.056	0.087	0.082

3.3. Secondary ion formation probability

The data in Fig. 7 can be used to correct the signal intensities of the spectra displayed in Fig. 4 for the apparent sampling efficiency and relate the resulting total signal of post-ionized neutral particles to that of the corresponding secondary ions. For that purpose, the signals of indium atoms and clusters were integrated over the relevant peaks in the SNMS and SIMS spectra displayed in Fig. 4, respectively. The SIMS signal was then corrected for the (baseline) background measured without primary ion and laser beam. The true LPI signal of sputtered post-ionized particles was evaluated from the SNMS spectrum and also corrected for the baseline, since no residual gas background peaks were detected at the relevant masses. The LPI signal determined this way was then corrected for the sampling efficiency determined above, and the relative ionization probability of the sputtered indium atoms and clusters was

Table 2
Ratio between integrated signals of In^+, In_2^+ or In_3^+ secondary ions and total summed signal of post-ionized neutral indium atoms or clusters, respectively. The values were calculated by multiplying the signal ratio evaluated from the mass spectra displayed in Fig. 4 with the respective relative sampling efficiency as described in the text.

	In	In_2	In_3
	In^+/In°	In_2^+/In_2°	In_3^+/In_3°
C_{60}	8.3×10^{-3}		
Ar_n	2.0×10^{-3}	3.1×10^{-3}	2.1×10^{-3}

calculated as the ratio between the secondary ion and the corrected post-ionized neutral signals. The resulting ion/neutral ratios are displayed in Table 2. While these values correctly reflect the variation of the ionization probability α^+ between the two different projectiles, their absolute magnitude is affected by the sampling correction factor υ mentioned above. Even though this introduces some uncertainty into the absolute ionization probability, it should be noted that the values determined here for argon cluster projectiles agree rather well with those measured under bombardment with 15-keV Xe^+ ions [23]. The fact that the ionization probability of In atoms is larger than that determined under gold cluster bombardment ($1–2 \times 10^{-4}$ [29]) is probably due to a residual oxygen contamination of the surface, since the data of ref [29] were measured on a dynamically sputter cleaned indium surface.

In any case, the data displayed in Table 2 can be used to compare the ionization probability between the two different projectile ion beams used here. It is evident that the ionization efficiency of the sputtered material is smaller under bombardment with gas cluster projectiles than under C_{60} bombardment. This is an interesting result, because it may reveal information about the electronic excitation generated by the projectile impact. One of the prevailing models describing secondary ion formation from a clean metal surface is the so-called substrate excitation model [46,47], which relates the excitation or ionization state of a sputtered particle to the transient electronic excitation of the surface generated by the projectile impact. In fact, computer simulations have shown that a significant part of the kinetic energy imparted by the projectile may transiently be dissipated via electronic degrees of freedom, for instance via electronic stopping of all moving particles which are set in motion in the course of a collision cascade, leading to relatively high electron temperature spikes which may boost the ionization of a sputtered atom or molecule [48–50]. An interesting open question in that context is whether the concerted impact of many atoms – as brought about by a cluster impact – can lead to a nonlinear enhancement of this electronic ionization. It is well known that clusters deposit their energy closer to the surface than iso-energetic atomic projectiles, leading to a high energy density in the immediate vicinity of the surface. As a consequence, cluster projectiles have been shown to produce a strong nonlinear enhancement of the sputter yield, meaning that the yield generated by a cluster impact is larger than that produced by its constituents impinging independently with the same impact velocity [41,51]. At present, it is still an open question whether a similar enhancement can be found for the electronic excitation. Although it is well known that secondary ion yields are drastically enhanced under cluster impact, this finding reflects enhancements of the partial sputter yield and/or the ionization probability. For sputtered indium atoms, these two effects have been disentangled by measuring the ionization probability of sputtered indium atoms as a function of the gold cluster projectile size [29]. As a result, it was found that α^+ remains essentially unchanged and – if at all - *decreases* with increasing size of the Au_n projectile, but the study was restricted to small clusters with $n \leq 5$. Larger cluster projectiles such as C_{60} were tried later [30], but the same order of magnitude (several 10^{-4}) was found for α^+ generated by 20-keV C_{60} impact. Since these projectiles induce chemistry at the irradiated surface, it was always desirable to repeat the same experiment with even larger rare gas clusters. The fact that the ionization probability measured here for 20 keV Ar_{1000} projectiles is smaller than that observed under C_{60} impact with the same kinetic energy clearly shows that there is no enhancement of the ionization probability under cluster bombardment.

Finally, however, it should be noted that gas cluster ion beams span a large range of parameters such as the nature of the cluster constituents, the cluster size and the energy per cluster constituent. For inert rare gas clusters, particularly the energy per atom may constitute a parameter that could in principle influence the ionization probability. Moreover, it is obvious that chemically reactive cluster projectiles such as, for instance, $(O_2)_n$ or $(H_2O)_n$ may lead to drastic ionization probability changes due to the chemical matrix effect. In that respect, further studies are clearly needed in order to fully explore the influence of the GCIB parameters on the secondary ion formation process.

4. Conclusions

Strong field laser post-ionization of sputtered neutral particles in combination with time-of-flight mass spectrometry allows to systematically investigate the ionization probability obtained in a SIMS experiment. Using a dual beam setup with two different cluster ion guns pointing at the same irradiated spot at the sample surface, one can utilize the same post-ionization conditions and directly compare the relative ionization efficiency achieved by different projectile ions by simply switching between the two ion beams. The results obtained for indium atoms and clusters sputtered from a polycrystalline indium surface as investigated here reveal that the large argon cluster projectile does not lead to an enhanced ionization efficiency of the emitted particles. In fact, the ionization probability measured under 20 keV Ar_{1000}^+ impact is found to be slightly smaller than that observed under iso-energetic C_{60} impact. Combined with previous data on cluster sputtering of indium, it is evident that the ionization probability of indium atoms sputtered from a clean indium surface is nearly independent of the nature, energy or nuclearity of the projectile. In contrast to the drastic nonlinear sputter yield enhancement found under cluster bombardment, this finding indicates that there is no such enhancement of the kinetic excitation induced by the projectile impact.

Acknowledgements

The authors acknowledge financial support of this research by the German Ministry of Science (BMBF) under grant 05K16PG1"Ion induced materials modification and characterization" as well as the Deutsche Forschungsgemeinschaft (DFG, German Research Foundation) - Projektnummer 278162697 - SFB 1242.

Appendix A. Supplementary data

Supplementary material related to this article can be found, in the online version, at doi:https://doi.org/10.1016/j.ijms.2018.12.007.

References

[1] N. Davies, D.E. Weibel, P. Blenkinsopp, N.P. Lockyer, R. Hill, J.C. Vickerman, Development and experimental application of a gold liquid metal ion source, Appl. Surf. Sci. 203 (2003) 223–227.
[2] A. Brunelle, S. la-Negra, J. Depauw, D. Jacquet, Y. Le Beyec, M. Pautrat, K. Baudin, H.H. Andersen, Enhanced secondary-ion emission under gold-cluster bombardment with energies from keV to MeV per atom, Phys. Rev. A 6302 (2001) 022902–022910.
[3] F. Kollmer, Cluster primary ion bombardment of organic materials, Appl. Surf. Sci. 231–2 (2004) 153–158.

[4] N. Wehbe, T. Mouhib, A. Delcorte, P. Bertrand, R. Moellers, E. Niehuis, L. Houssiau, Comparison of fullerene and large argon clusters for the molecular depth profiling of amino acid multilayers, Anal. Bioanal. Chem. 406 (2014) 201–211.
[5] D. Rading, R. Moellers, F. Kollmer, W. Paul, E. Niehuis, Dual beam depth profiling of organic materials: variations of analysis and sputter beam conditions, Surf. Interf. Anal. 43 (2011) 198–200.
[6] D. Touboul, F. Kollmer, E. Niehuis, A. Brunelle, O. Laprevote, Improvement of biological time-of-flight-secondary ion mass spectrometry imaging with a bismuth cluster ion source, J. Am. Soc. Mass Spectr. 16 (2005) 1608–1618.
[7] R. Kersting, B. Hagenhoff, F. Kollmer, R. Mollers, E. Niehuis, Influence of primary ion bombardment conditions on the emission of molecular secondary ions, Appl. Surf. Sci. 231–232 (2004) 261–264.
[8] D.E. Weibel, S. Wong, N.P. Lockyer, P. Blenkinsopp, R. Hill, J.C. Vickerman, A C_{60} primary ion beam system for time of flight secondary ion mass spectrometry: its development and secondary ion yield characteristics, Anal. Chem. 75 (2003) 1754–1764.
[9] N. Toyoda, J. Matsuo, T. Aoki, I. Yamada, D.B. Fenner, Secondary ion mass spectrometry with gas cluster ion beams, Appl. Surf. Sci. 203 (2003) 214–218.
[10] R. Hill, P. Blenkinsopp, S. Thompson, J. Vickerman, J.S. Fletcher, A new time-of-flight SIMS instrument for 3D imaging and analysis, Surf. Interf. Anal. 43 (2011) 506–509.
[11] S. Kayser, D. Rading, R. Moellers, F. Kollmer, E. Niehuis, Surface spectrometry using large argon clusters, Surf. Interf. Anal. 45 (2013) 131–133.
[12] N. Winograd, The magic of cluster SIMS, Anal. Chem. 77 (2005) 142A–149A.
[13] S. Ninomiya, Y. Nakata, Y. Honda, K. Ichiki, T. Seki, T. Aoki, J. Matsuo, A fragment-free ionization technique for organic mass spectrometry with large Ar cluster ions, Appl. Surf. Sci. 255 (2008) 1588–1590.
[14] S.R. Coon, W.F. Calaway, J.W. Burnett, M.J. Pellin, D.M. Gruen, D.R. Spiegel, J.M. White, Yields and kinetic energy distributions of sputtered neutral copper clusters, Surf. Sci. 259 (1991) 275–287.
[15] S.R. Coon, W.F. Calaway, M.J. Pellin, J.M. White, New findings on the sputtering of neutral metal clusters, Surf. Sci. 298 (1993) 161–172.
[16] A. Wucher, M. Wahl, H. Oechsner, Sputtered neutral silver clusters up to Ag_{18}, Nucl. Instrum. Methods B 82 (1993) 337–346.
[17] M. Wahl, A. Wucher, VUV photoionization of sputtered neutral silver clusters, Nucl. Instrum. Methods B 94 (1994) 36–46.
[18] Z. Ma, S.R. Coon, W.F. Calaway, M.J. Pellin, D.M. Gruen, E.I. Nagy-Felsobuki, Sputtering of neutral and ionic indium clusters, J. Vac. Sci. Technol. 12 (1994) 2425–2430.
[19] S.R. Coon, W.F. Calaway, M.J. Pellin, Neutral copper cluster sputtering yields: Ne^+, Ar^+ and Xe^+ bombardment, Nucl. Instrum. Methods B 90 (1994) 518–522.
[20] A. Wucher, M. Wahl, The formation of clusters during ion induced sputtering of metals, Nucl. Instrum. Methods B 115 (1996) 581–589.
[21] C. Staudt, R. Heinrich, A. Wucher, Formation of large clusters during sputtering of silver, Nucl. Instrum. Methods B 164–165 (2000) 677–686.
[22] A. Wucher, Formation of clusters in sputtering, Izv. Akad. Nauk. Ser. Fiz. 66 (2002) 499–508.
[23] C. Staudt, A. Wucher, Generation of large indium clusters by sputtering, Phys. Rev. B 66 (2002), 075419-075411.
[24] P.G. Thirolf, D. Habs, M. Gross, K. Allinger, J. Bin, A. Henig, D. Kiefer, Laser particle acceleration: status and perspectives for nuclear physics, Acta Phys. Pol. B 42 (2011) 843–852.
[25] A. Samartsev, A. Wucher, Yields and ionization probabilities of sputtered Inn particles under atomic and polyatomic Au_m^- ion bombardment, Appl. Surf. Sci. 252 (2006) 6474–6477.
[26] B. Czerwinski, R. Samson, B.J. Garrison, N. Winograd, Z. Postawa, Desorption of organic overlayers by Ga and C_{60} bombardment, Vacuum 81 (2006) 167–173.
[27] Z. Postawa, B. Czerwinski, M. Szewczyk, E.J. Smiley, N. Winograd, B.J. Garrison, Microscopic insights into the sputtering of Ag{111} induced by C_{60} and Ga bombardment, J. Phys. Chem. B 108 (2004) 7831–7838.
[28] S. Sun, C. Szakal, E.J. Smiley, Z. Postawa, A. Wucher, B.J. Garrison, N. Winograd, Sputtering of Ag under C_{60}^+ and Ga^+ projectile bombardment, Appl. Surf. Sci. 231–232 (2004) 64–67.
[29] A.V. Samartsev, C. Heuser, A. Wucher, Ionization probabilities of sputtered indium atoms under atomic and polyatomic Au_m- ion bombardment, Surf. Interface Anal. 45 (2012) 87–89.
[30] L. Breuer, A. Kucher, M. Herder, A. Wucher, N. Winograd, Formation of neutral In_nC_m clusters under C_{60} ion bombardment of indium, J. Phys. Chem. A 118 (2014) 8542-.
[31] R.M. Braun, P. Blenkinsopp, S.J. Mullock, C. Corlett, K.F. Willey, J.C. Vickerman, N. Winograd, Performance characteristics of a chemical imaging time-of-flight mass spectrometer, Rapid Commun. Mass Spectr. 12 (1998) 1246–1252.
[32] A. Wucher, Laser postionization - fundamentals, in: J.C. Vickerman, D. Briggs (Eds.), TOF-SIMS: Materials Analysis by Mass Spectrometry, IM Publications and SurfaceSpectra, 2013, pp. 217–246.
[33] A. Kucher, A. Wucher, N. Winograd, Strong-field ionization of beta-estradiol in the IR: strategies to optimize molecular postionization in secondary neutral mass spectrometry, J. Phys. Chem. C 118 (2014) 25534–25544.
[34] G. Gingras, A. Tripathi, B. Witzel, Wavelength and intensity dependence of short pulse laser xenon double ionization between 500 and 2300 nm, Phys. Rev. Lett. 103 (2009), 173001.
[35] A. Pelster, M. Körsgen, M. Heeger, H.F. Arlinghaus, Implementation and optimization of large gas cluster laser post-ionization secondary neutral mass spectrometry for molecular analysis, J. Phys. Chem. C 121 (2017) 15266–15271.
[36] S.M. Hankin, D.M. Villeneuve, P.B. Corkum, D.M. Rayner, Nonlinear ionization of organic molecules in high intensity laser fields, Phys. Rev. Lett. 84 (2000) 5082–5085.
[37] R. Heinrich, A. Wucher, Projectile size effects on cluster formation in sputtering, Nucl. Instrum. Methods B 207 (2003) 136–144.
[38] R. Heinrich, A. Wucher, Self sputtering of silver using polyatomic projectiles, Nucl. Instrum. Methods B 193 (2002) 781–786.
[39] A. Samartsev, A. Wucher, Sputtering of indium using polyatomic projectiles, Appl. Surf. Sci. 231–232 (2004) 191–195.
[40] A. Samartsev, A. Duvenbeck, A. Wucher, Sputtering of indium using Au_m projectiles: transition from linear cascade to spike regime, Phys. Rev. B 72 (2005) 1–10.
[41] H.H. Andersen, Nonlinear effects in collisional sputtering under cluster impact, in: P. Sigmund (Ed.), Fundamental Processes in Sputtering of Atoms and Molecules (SPUT 92), Det Kongelige Danske Videnskabernes Selskab, Copenhagen, 1993, pp. 127–153.
[42] N.J. Popczun, L. Breuer, A. Wucher, N. Winograd, On the SIMS ionization probability of organic molecules, J. Am. Soc. Mass Spectr. 28 (2017) 1182–1191.
[43] N.J. Popczun, L. Breuer, A. Wucher, N. Winograd, ionization probability in molecular secondary ion mass spectrometry: protonation efficiency of sputtered guanine molecules studied by laser postionization, J. Phys. Chem. C 121 (2017) 8931–8937.
[44] D. Maciazek, M. Kanski, L. Gaza, B.J. Garrison, Z. Postawa, Computer modeling of angular emission from Ag(100) and Mo(100) surfaces due to Ar-n cluster bombardment, J. Vac. Sci. Technol. B 34 (2016).
[45] L. Rzeznik, R. Paruch, B.J. Garrison, Z. Postawa, Sputtering of a coarse-grained benzene and Ag(111) crystals by large Ar clusters – effect of impact angle and cohesive energy, Surf. Interface Anal. 45 (2013) 27–30.
[46] Z. Sroubek, J. Lorincik, Ionization and excitation processes in sputtering in the light of the experimental evidence, Surf. Rev. Lett. 6 (1999) 257–264.
[47] A. Wucher, B. Weidtmann, A. Duvenbeck, A microscopic view of secondary ion formation, Nucl. Instrum. Methods B 303 (2013) 108–111.
[48] A. Duvenbeck, Computer Simulation of Electronic Excitation in Atomic Collisional Cascades, Fachbereich Physik, Universität Duisburg-Essen, Duisburg, 2007.
[49] A. Duvenbeck, Z. Sroubek, A. Wucher, Electronic excitation in atomic collision cascades, Nucl. Instrum. Methods B 228 (2005) 325–329.
[50] A. Wucher, A. Duvenbeck, Kinetic excitation of metallic solids: progress towards a microscopic model, Nucl. Instrum. Methods B 269 (2011) 1655–1660.
[51] S. Bouneau, A. Brunelle, S. Ia-Negra, J. Depauw, D. Jacquet, Y. Le Beyec, M. Pautrat, M. Fallavier, J.C. Poizat, H.H. Andersen, Very large gold and silver sputtering yields induced by keV to MeV energy Au/sub n/ clusters (n=1-13), Phys. Rev. B 65 (2002) 144106–144108.